Temperature-Adaptive Ultralubricity of a WS2/a-C Nanocomposite Coating

Cao, Huatang; Momand, Jamo; Syari'Ati, Ali; Wen, Feng; Rudolf, Petra; Xiao, Ping; De Hosson, Jeff Th M.; Pei, Yutao

Published in:
ACS Applied Materials and Interfaces

DOI:
10.1021/acsami.1c06061

Publication date:
2021

ACS APPLIED MATERIALS & INTERFACES

www.acsami.org

Research Article

Temperature-Adaptive Ultralubricity of a WS_2/a-C Nanocomposite Coating: Performance from Room Temperature up to 500 °C

Huatang Cao,* Jamo Momand, Ali Syari'ati, Feng Wen, Petra Rudolf, Ping Xiao,* Jeff Th. M. De Hosson, and Yutao Pei

Cite This: *ACS Appl. Mater. Interfaces* 2021, 13, 28843−28854

Read Online

ACCESS | Metrics & More | Article Recommendations | Supporting Information

ABSTRACT: This study reports on the ultralubricity of a high-temperature resilient nanocomposite WS_2/a-C tribocoating. The coefficient of friction of this coating remains at around 0.02 independently of a thermal treatment up to ~500 °C, as confirmed by high-temperature tribotests. Moreover, the coating annealed at 450 °C keeps exhibiting a similar ultralubricity when cooled back down to room temperature and tested there, implying a tribological self-adaptation over a broad temperature range. High-resolution TEM observations of the tribofilms on the wear track unveil that WS_2 nanoplatelets form dynamically via atomic rearrangement and extend via unfaulting geometrical defects (bound by partial climb dislocations). The (002) basal planes of the WS_2 nanoplatelets, reoriented parallel to the tribo-sliding direction, contribute to a sustainable ultralubricity. The declining triboperformance beyond 500 °C is associated with sulfur loss rather than the transformation of WS_2 into inferior WO_3 via oxidation as suggested earlier. This self-adaptive WS_2/a-C tribocoating holds promise for a constant ultralubrication with excellent thermal performance.

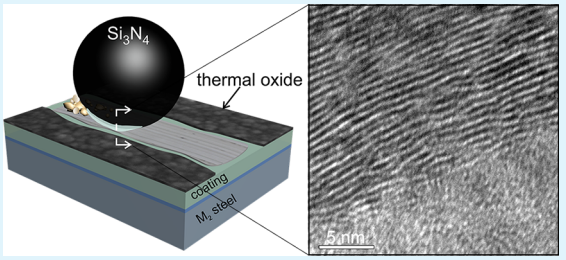

KEYWORDS: *WS_2, chameleon coating, self-adaptation, ultralubricity, high temperature, oxidation*

1. INTRODUCTION

Adaptive chameleon-like tribocoatings are a new class of smart materials that are designed to adjust their surface chemical composition and structure in response to dynamic changes in the working environment.[1,2] Such coatings exhibit automatic structural and chemical self-adaptations to the ambient multienvironments (e.g., vacuum, dry−humid air, and room-elevated temperature) to reduce friction and wear over extended ranges of cycled environmental conditions. The surface chemistry of adaptive tribocoatings dynamically transforms in contact areas to produce specific lubricious phases in response to an immediate operational environment.[1] Such chameleon-like tribocoatings could promote aerospace innovations that were previously frustrated by the lack of available lubricants capable of functioning in extreme environments.

For high-temperature tribological applications, there are many candidate materials,[3−5] such as layered transition-metal dichalcogenides (TMDCs, e.g., MoS_2, WS_2, and $MoSe_2$), graphite, and amorphous diamond-like carbon (DLC or a-C) films,[6−10] which have been reported to operate functionally with the lowest friction and wear rates generally below 300 °C but lose their lubricating characteristics at higher temperatures because of oxidation-induced degradation.[10−13] Some other temperature-adaptive lubricating materials allowing for diffusion-based and/or oxidation-based mechanisms can be potentially used over multiple thermal cycles in microlaminate architectures;[1,5,11,13−18] their metal or transition-metal suboxides including the so-called Magnéli phases (e.g., TiO_x, MoO_x, VO_x, and WO_x) are suitable as middle temperature range lubricants.[11,12,19,20] Ceramic-enhanced coatings (particularly when comprising Ag) have been found to further lift the temperature threshold; yet, they generate higher coefficient of frictions (CoFs) (>0.2−1).[13,16,17,21,22]

Moreover, most tribocoatings are temperature dependent and thus only offer lubrication in a certain range of elevated temperature.[23−25] For instance, both the first-generation temperature-adaptive PbO−MoS_2 coatings and a YSZ−Ag−Mo−MoS_2 coating developed in the following become abrasive after heating.[1] Similarly, some binary compounds such as CuO−MoO_3 and Ag_2O−MoO_3 can produce lubricious double oxides over the range of 25−800 °C[26,27] but fail to maintain ultralubricity when the surface is cooled to room temperature because of the formation of abrasive oxidized compounds. Thus, one major hurdle in these chameleon-like tribocoatings is the reversibility of their lubrication over multienvironmental cycles.

Received: April 1, 2021
Accepted: May 27, 2021
Published: June 8, 2021

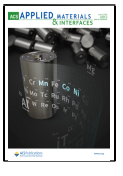

Up to now, the high-temperature tribological behavior has been mainly evaluated at discrete temperatures, while few coatings can survive well through a temperature ramp heating. For instance, a TiC/a-C:H nanocomposite coating that is thermally stable to 350 °C failed at a much lower ramping temperature of 210 °C,[28] and MoCN−Ag coatings exhibited a rather unstable frictional behavior during ramping to 700 °C.[15,24] Thus, the hypothesis that the coatings show a stably low CoF over a broad temperature range has still not been sufficiently validated.

Therefore, self-adaptive coatings with thermally reversible surface chemistry and sustained ultralubricity in a broad temperature range are in urgent demand. Among appealing lubricants, WS_2 surpasses others owing to its unique anisotropic crystal structure, i.e., hexagonal units wherein layers of tungsten atoms are sandwiched in-between layers of sulfur atoms. The W−S bond in one sheet is covalent, but different sheets are stacked by weak Van der Waals forces. One of the favorable properties invariably connected to WS_2 is that the crystal is easily cleaved and sheared (τ = 1−2 MPa) between the (002) basal layers.[1] Materials shearing readily at high temperatures are abrasive under the conditions where TMDCs are unparalleled as solid lubricants.[1] This implies that the high-temperature tribocapacity of WS_2-based coatings is still far from being fully exploited. The mechanical properties of WS_2 can be further tailored by introducing a compliant amorphous carbon (a-C) matrix to generate a high density of interphase regions that lend support to crack deflection, cessation of columnar growth, and protect WS_2 from oxidations.[29] This study reports on the synthesis, the ultralubricity, and failure mechanism of a WS_2/a-C coating that self-adapts to temperature changes and has the potential to provide steady high-temperature ultralubrication for aerospace applications.

2. EXPERIMENTAL DETAILS

2.1. Preparation of the WS/a-C Coating. Nanocomposite WS_2/a-C coatings were deposited on both single crystal silicon (100) wafers (525 ± 25 μm thickness) and M_2 high-speed steel (HSS) via a TEER UDP400/4 closed-field unbalanced magnetron sputtering system. The coatings on silicon wafers were prepared for microstructure observations, and the ones on HSS were made for high-temperature tribotests. The sputtering system was configured with one Cr target (99.5% purity), one graphite target (99.99% purity), and two WS_2 targets (99.9% purity) opposite to each other in the Ar plasma. The two magnetrons for the Cr and graphite targets were powered by a Pinnacle 6/6 kW double-channel DC power supply (Advanced Energy), and the other two magnetrons for the WS_2 targets were powered by a Pinnacle Plus 5/5 kW double-channel pulsed DC (p-DC) power supply (150 kHz, 70% duty cycle, Advanced Energy). All of the power supplies for sputtering were operated in the current control mode and set at 0.5 A (1.5 A) for the WS_2 (graphite) targets. The substrates were ultrasonically cleaned in acetone three times before being mounted vertically on a carousel holder rotating at 3 rpm in front of the targets and then subjected to Ar plasma etching for 20 min at −400 V bias voltage (p-DC mode, 250 kHz, and 87.5% duty cycle) to remove surface contamination. A ∼300 nm thick Cr interlayer was first deposited to facilitate the interfacial adhesion between the coating and substrate. The coating was about 2 μm thick. The base pressure of the chamber prior to deposition was 3−5 × 10^{-4} Pa. No additional substrate heating was applied during deposition.

2.2. Characterization of the WS_2/a-C Coating. Thermogravimetric analysis (TGA) was conducted on a TGA/SDTA851e Analyzer (Mettler-Toledo). The samples were heated in an Al_2O_3 crucible from 30 to 800 °C at a heating rate of 10 °C min^{-1} under a flow of air and N_2, respectively (30 mL min^{-1}). Energy-dispersive X-ray spectroscopy (EDS, Octane Silicon Drift Detector, EDAX) with an accelerating voltage of 20 kV in a Philips XL30 E-SEM was employed to estimate the chemical composition of the coatings before and after annealing treatment. EDS results were averaged by accumulating the signal from the same spot size (1000× magnification) for 100 s; three spots were randomly chosen on each sample.

The grazing incidence X-ray diffraction (GI-XRD) spectra were collected from 5° to 80° with a PANalytical X'Pert MRD diffractometer to determine the phases of the coatings, using 2° incident angle in parallel beam geometry with a step size of 0.0025° and a collection time of 100 s per step. Raman spectra on the wear tracks were acquired with a Thorlabs HNL setup equipped with a HeNe laser (632.8 nm) at 1−2 mW power in the range of 200−2000 cm^{-1}; each spectrum was the sum of 100 scans.

X-ray photoelectron spectroscopy (XPS) was employed to investigate the surface stoichiometry and gain insight into the types of chemical bonds present in the coatings after different treatments; we used a Surface Science SSX-100 ESCA instrument with a monochromatic Al Kα X-ray source ($h\nu$ =1486.6 eV). During data acquisition, the pressure in the measurement chamber was kept at 2 × 10^{-7} Pa. The electron take-off angle with respect to the surface normal was 37°; the analyzed area was 1000 μm in diameter, and the total energy resolution was 1.16 eV. The XPS spectra were analyzed using the least-squares curve-fitting program (Winspec, developed at the LISE laboratory of the University of Namur, Namur, Belgium). Deconvolution of the spectra included a Shirley background subtraction and fitting with a minimum number of peaks consistent with the chemical structure of the sample. The uncertainty in the peak intensity determination was 2% for the core levels reported.

The hardness and elastic modulus of the composite coatings were measured by the MTS Nano indenter XP equipped with a Berkovich diamond tip. The indentation depth was fixed at 200 nm, i.e., to approximately 10% of the coating thickness, to avoid the influence of the substrate. Tribotests were run for 5000 laps (unless catastrophic failure occurred) using a pin-on-disk high-temperature tribometer (CSM Instruments) against a Φ6 mm Si_3N_4 ceramic ball; the high-temperature tests were conducted in ambient air (relative humidity, R_H, 55%) with the sliding speed set to 10 cm s^{-1} (wear track diameter of 15−18 mm) under a normal load of 5 N. For comparison, the tribological performance of the same coating at room temperature was examined in dry air (R_H, 5−7%) and humid air (R_H, 55%) against the Φ6 mm 100Cr6 steel ball at 5 N load.

A focused ion beam (FIB, FEI Helios G4) microscopy was employed to slice a TEM lamella at the center of the wear track in situ tribotested at the temperature of 450 °C and of the sample preannealed at the 450 °C for 1 h in air to compare the oxidation effects. Before milling, two protective Pt layers were deposited using electron and ion beams sequentially to reduce the Ga ion irradiation damage on the top surface of interest. The microstructure of the coating, tribofilms, and wear tracks was investigated by analytical high-resolution transmission electron microscopy (HR-TEM, JEOL 2010F-FEG, operated at 200 kV), scanning electron microscopy (SEM, Philips XL30 E-SEM), and optical microcopy (Olympus VANOX-T).

3. RESULTS

3.1. Microstructure. Figure 1 shows the microstructure of the as-deposited WS_2/a-C coating, which exhibits ultrashort (2−3 nm) WS_2 nanocrystallites randomly distributed in an amorphous carbon (a-C) matrix. The diffraction halo in the selective area electron diffraction (SAED) pattern (inset of Figure 1) confirms the primarily amorphous nature of the composite coating because of a relatively high carbon content (C: 34.2 atom %; O: 2.3 atom %; S: 35.9 atom %; W: 37.6 atom %, see Table 1).

https://doi.org/10.1021/acsami.1c06061
ACS Appl. Mater. Interfaces 2021, 13, 28843−28854

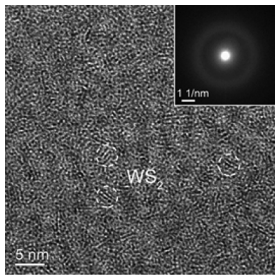

Figure 1. HR-TEM image showing the amorphous character of the as-deposited WS_2/a-C coating: ultrashort WS_2 nanoplatelets are randomly distributed in an amorphous carbon matrix. The inset with the SAED pattern shows a halo ring.

3.2. Tribological Behavior. Figure 2a shows that the coating has both low CoFs in humid air (0.098) and dry air (0.021) at room temperature, and the corresponding lubrication mechanisms under these same conditions were detailed in elsewhere.[29−31] A striking result is displayed in Figure 2b, which shows the tribological behavior under continuously ramping heating process from 100 to 500 °C. The CoF remains lower than 0.02 (even lower than that in room-temperature testing shown in Figure 2a) over the whole temperature range, evidencing a chameleon tribological response independent of the thermal treatment. In particular, in the temperature range of 150−200 °C, the CoF even reaches values indicative of superlubrication (<0.01).

Concerning triboapplications at high temperatures, Figure S1 shows the triboperformance at 100, 200, 400, 450, 500, and 600 °C. The CoF at 100 °C (where water molecules evaporate) over 5000 sliding cycles is 0.043. Heating to temperatures above 100 °C will lead to drying of the atmosphere around the testing pin, thereby ruling out the detrimental effect of humidity in increasing the friction, and one hence expects a lower CoF than 0.1 deduced under humid conditions (55% R_H) from the room temperature data shown in Figure 2a. The CoF further decreases to 0.016 at 200 °C and then stabilizes at around 0.02 at both 400 and 450 °C. For an even higher temperature (500 °C), the coating also has an ultralow initial CoF of below 0.02 during the first 1500 sliding laps. However, CoF starts to increase to 0.1 at around 2000 laps, and after 3000 laps, the CoF further rises to 0.6, which is deemed as a failure for DLC-based coatings owing to a direct metal contact. At 600 °C, the coating exhibits an instant catastrophic failure in <30 laps. Figure S2 shows the SEM micrographs of the morphology of wear tracks tested at 100, 200, 400, and 450 °C: at 100 and 200 °C, the wear tracks are very superficial, with some thin tribofilms adhering tightly to the wear tracks. In the wear track of the sample tested at 400 °C, some bubbles or peel-off can be observed. The wear track becomes deeper at 450 °C, and even thicker top tribolayers are

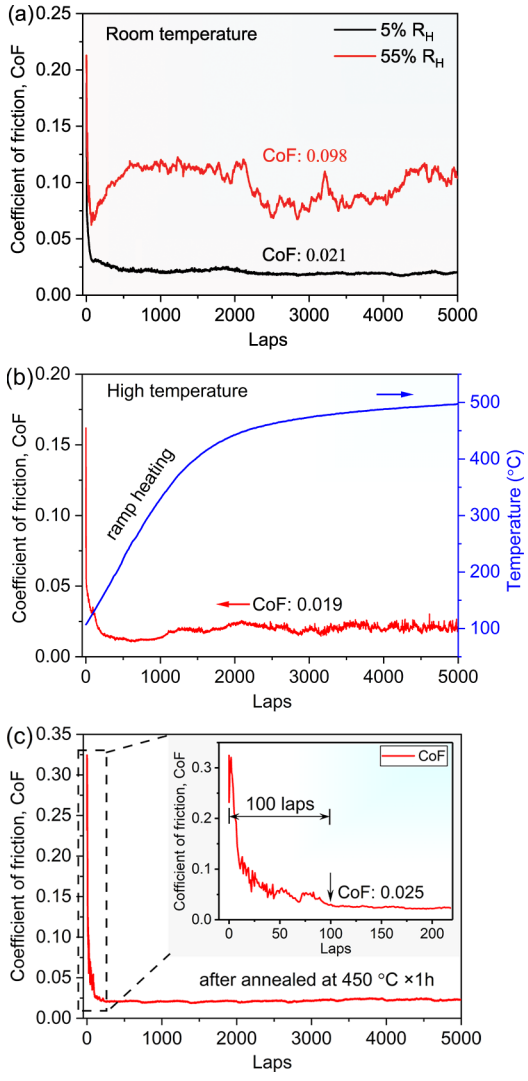

Figure 2. Tribological performance of the WS_2/a-C coating under different testing conditions: (a) tested at room temperature in dry air (5% R_H) and ambient air (55% R_H) for comparison, (b) tested while continuously increasing the temperature from 100 to 500 °C in ambient air (55% R_H), and (c) tested at room temperature in dry air (5% R_H) with the WS_2/a-C coating annealed at 450 °C for 1 h. The insert reveals an ultralow CoF < 0.025 achieved after only 100 laps and maintained for 5000 laps.

Table 1. Chemical Composition of WS_2/a-C Coatings before and after Annealing to Different Temperatures as Deduced from EDS analysis

sample no.	composition (atom %)				S/W	decomposition rate[a]
	C	O	S	W		
as-deposited coating	34.2 ± 0.5	2.3 ± 0.5	35.9 ± 0.5	27.6 ± 0.5	1.30	
annealed at 200 °C	34.6 ± 0.8	2.5 ± 0.5	35.5 ± 0.6	27.4 ± 0.5	1.30	1.1%
annealed at 400 °C	25.3 ± 0.8	24.0 ± 0.5	25.3 ± 0.5	25.4 ± 0.6	0.99	29.6%
annealed at 450 °C	25.7 ± 0.5	25.5 ± 0.5	25.8 ± 0.5	23.0 ± 0.5	1.12	28.2%
annealed at 500 °C	8.0 ± 1.2	52.2 ± 1.0	1.6 ± 0.5	38.2 ± 1.1	0.04	95.5%
annealed at 600 °C	6.5 ± 0.7	53.5 ± 1.0	1.4 ± 0.5	38.6 ± 0.6	0.04	96.1%

[a]The decomposition rate is based on the loss of S.

https://doi.org/10.1021/acsami.1c06061
ACS Appl. Mater. Interfaces 2021, 13, 28843−28854

found closer to the wear edges (see Figure S2h). Figure S2 confirms that all the coatings survive and stay intact during tribo-sliding below 450 °C, but the coating fails after sliding 3000 laps when tested at 500 °C, and it immediately fails when tested at 600 °C. Figure S3 shows that the residual coating is fractured after testing at 500 °C (>3000 laps) in both the untouched regions and the wear track, indicating coating failures. Thus, it can be concluded that the WS_2/a-C coating can tribologically survive intact up to a temperature of ∼450 °C, which is much higher than the reported degrading temperature of a sputtered pure WS_2 film of 300 °C.[12]

To evaluate the thermal damage tolerance, the coating annealed at 450 °C for 1 h in air was tribotested, and the result is shown in Figure 2c. The same level of ultralow CoF of 0.025 was reached after sliding 100 laps and maintained thereafter. In particular, the ultralow steady-state CoFs measured over 5000 laps (see Figure 2b,c) suggest that the oxides formed on the surface during the thermal treatment do not degrade the tribological properties. It should be pointed out that the thickness of the oxides is estimated much larger for the postannealed sample (450 °C for 1 h) than those tribotested continuously in situ because of wear, but they all exhibit similar tribological behavior (all CoFs are close to 0.02, as shown in Figures S1a−d and 2b,c). In fact, the SEM images of the wear track of a WS_2/a-C coating annealed at 450 °C for 1 h in Figure 3 show that loose parts of the coating, which apparently formed during the annealing, slide away rapidly (<100 laps), and a thin adhesive tribofilm seems to have dynamically accumulated in the center of the wear track (Figure 3c), similar to what was observed during in situ tests (see Figure S2).

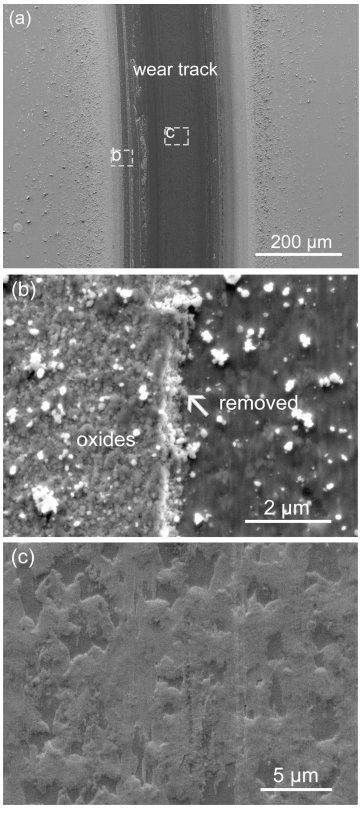

Figure 3. SEM image of the wear track of a WS_2/a-C coating annealed at 450 °C for 1 h: (a) low-magnification overview, (b) the close-up view of the side edge of the wear track shows debris accumulated during the test, and (c) the center part of the wear seems to dynamically accumulate a tribofilm.

In summary, Figures 2, 3, S1, and S2 present evidence for a tribological adaptation of WS_2/a-C nanocomposite coating to temperature changes in a wide range of 25−450 °C and maintaining an ultralow CoF of ∼0.02.

4. DISCUSSION

From Figure 4, where the highlighted CoFs deduced from our tribotests are compared with the literature data of tests performed at temperatures spanning from 25 to 800 °C, we can deduce that the high-temperature triboperformance up to 500 °C of the present WS_2/a-C coating investigated here is probably superior to all tribocoatings reported so far.[6−9,11,13−22,28,32]

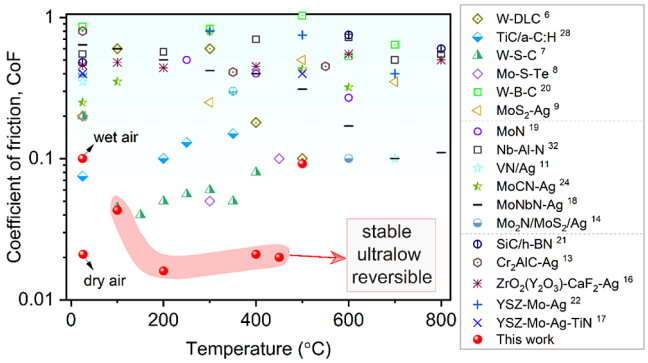

Figure 4. Comparisons of CoFs of this work with the literature on tribotests performed at temperatures spanning from 25 to 800 °C: the WS_2/a-C coating (see highlighted values) exhibits ultralow CoFs from 25 °C (dry air) to 500 °C. Note that 100 °C is a critical temperature for removing the effect of humidity, and CoF jumps to >0.1 after 2000 laps of sliding at 500 °C for the investigated WS_2/a-C coating.

The key question is what is the real driving force for such a good triboperformance of the WS_2/a-C coating both during a ramped up heating and after annealing to 450 °C. To achieve adaptive reversibility over temperature cycles, one conventional route is to introduce a multilayered microarchitecture[17] to ensure that some lubricious phase is preserved in its as-deposited state for later replenishing; this clearly does not apply to the homogeneous isotropic WS_2/a-C nanocomposite coating here. Hence, new lubricating mechanisms must be at play and three points remain to be answered in this study:

- How is the reversibility adaptation to elevated temperatures achieved in the coating?
- Why does the coating fail to function above 500 °C?
- Why is an ultralow CoF of 0.02 maintained during the whole sliding process?

4.1. Reversible Triboadaptation to Temperature Change. To unravel the microstructure evolution of the tribofilm formed in different areas on the wear track of the WS_2/a-C coating after tribotesting at 450 °C (see Figure S2g,h), a TEM lamella was prepared by cutting across the border of the areas A and B, as illustrated in Figure 5a. Figure 5b shows the overview of the cross-sectional lamella, presenting a tribofilm with variable thickness formed on the wear track. The close-up views of the cross section of areas A and B, shown in Figure 5c,d, respectively, reveal that the flat area A is covered by a thin layer of tribofilm (20−50 nm),

https://doi.org/10.1021/acsami.1c06061
ACS Appl. Mater. Interfaces 2021, 13, 28843−28854

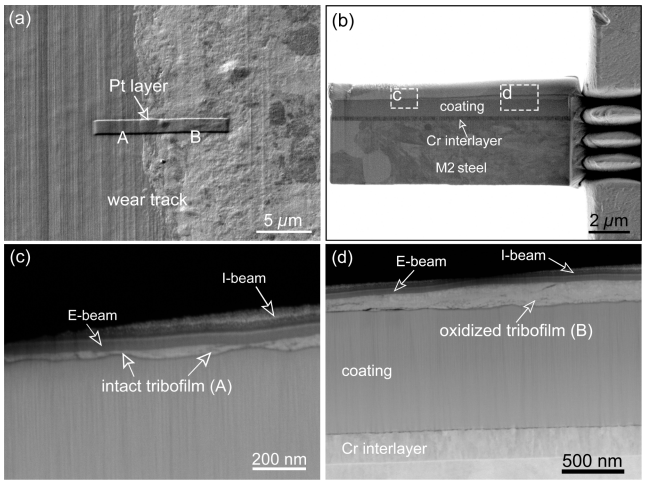

Figure 5. SEM images of a TEM lamella cut with a FIB from the wear track of a WS_2/a-C coating tribotested at 450 °C: (a) location and (b) overview of the TEM lamella. Cross-sectional close-up views of (c) the flat area A with an intact tribofilm and (d) the uneven area B with an oxidized tribofilm marked in (a). Note that before FIB slicing, protective Pt layers were deposited by electron beam and ion beam sequentially to avoid damage.

while the uneven area B presents a much thicker tribofilm (up to ∼200 nm).

Figure 6a presents the overview HR-TEM image of area A in Figure 5 and confirms that the tribofilm formed on the A area

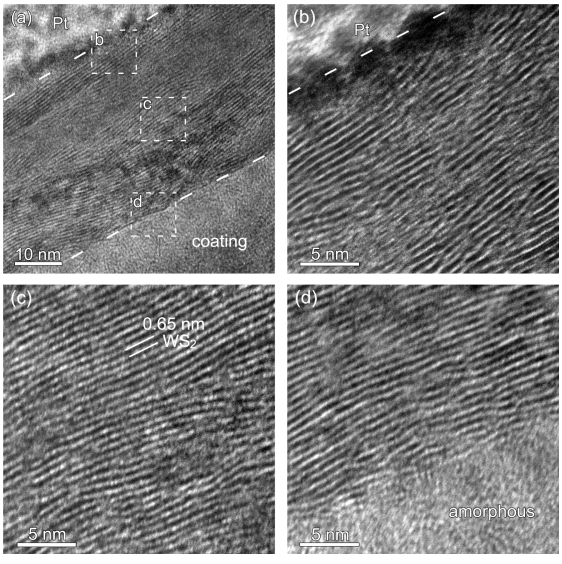

Figure 6. Cross-sectional HR-TEM images of the intact tribofilm formed on the flat area A marked in Figure 5a revealing a full reorientation of WS_2(002) basal planes parallel to the sliding direction: (a) overview of the tribofilm and (b–d) close-up view of the top, middle, and bottom region, respectively, as marked in (a).

of the wear track (tested at 450 °C) is about 40 nm thick, with no voids or cavities at the interface between the tribofilm and the untouched part of the coating. Figure 6b–d shows the close-up views of the top, center, and bottom region of the tribofilm; all show extended crystalline WS_2(002) planes that are perfectly parallel to the sliding direction. The interlamellar *c*-plane spacing between the WS_2 planes in Figure 6c was ∼6.5 Å, which is slightly larger than the indexed 6.18 Å lattice spacing of WS_2(002) basal planes (JCPDS no. 008-0237), indicating that the WS_2 layers are slightly expanded.[33] Note that such thick, long-range, almost fully well-aligned WS_2 platelets have rarely been reported in earlier studies,[5,34] where most often only a few nanometer thick layers of such platelets were observed. In addition, previous studies[35,36] suggested that amorphous TMDC platelets gradually crystallize from the bottom of the wear track and only become fully crystalline in the outmost part of the tribofilm in direct contact with the counterpart; in other words, these works describe a gradient of crystallinity in the layer, from amorphous to crystalline. In contrast, Figure 6a shows a predominantly crystalline tribofilm throughout its entire thickness of about 40 nm on top of the unaffected amorphous coating. In particular, Figure 6d gives evidence for WS_2(002) basal planes aligned with the sliding direction directly at the interface. We can therefore speculate that the formation of such aligned platelets, which must have taken place during an extremely short running-in period, is responsible for the rapid decrease in the CoF from >0.1 to 0.02 (see Figure S1d). Put differently, the coating reacts with an instant self-adaptive tribological response to the high-temperature sliding under frictional contact by forming lubricating tribolayers.

The HR-TEM images in Figure 7 present instead the microstructure of tribofilms in the uneven area B marked in Figure 5a. The 200 nm thick tribofilm shown here was thermally oxidized: Figure 7a shows that in the top part, WO_3(002) planes with a *d*-spacing of 3.8 Å tend to be nearly parallel to the sliding direction, similarly as the WS_2(002) planes, which can also be distinguished in the micrograph. Note that the transition-metal oxides such as WO_3, W_xO_{3x-1}, and W_xO_{3x-2} also possess a layered structure and are recognized as potential solid lubricants (CoF about 0.2–0.3),[12,37−39] although less effective than WS_2 (<0.05) in vacuum or dry air. For instance, for a Ti–WS_2 film tested in humid ambient air, Scharf et al.[12] ascribed the CoF of 0.18 as approximately halfway between pure WS_2 (∼0.1) and WO_3 (0.3).

Figure 7b shows a mixture of WS_2 and WO_3 nanocrystallites, indicating that the tribofilm is partially oxidized. However, the average CoF measured at 450 °C (and also at the early stage of testing at 500 °C) in this study was surprisingly low, 0.02 (see Figure S1d,e), suggesting that the WS_2 phase is the main contributor to the ultralubricative behavior below 500 °C. In contrast, the tribo/thermal oxidation-induced WO_3 phase played a minor role as no worsening of the CoF was observed. In fact, Figure 3b proves that thick, loosely bonded thermal oxide is removed rapidly from the wear track, and new WS_2 arising from the bulk coating appears to restock the lubricants (Figure 3c).

It should be noted that the initial partial oxidation and successive removal of the oxidized phase are a dynamic process throughout the continuous sliding at 450 °C, i.e., the oxidation of the top layer and its removal proceed simultaneously as testified to by some sudden intermittent spikes in the CoF curve up to 0.045 followed by rapid drops to low values again <0.02 during ∼900 sliding laps (Figure S1d). These spikes indicate that thin oxidized layers that slightly increase the friction are temporarily present. Moreover, Figure 7c shows that also WO_3 with perpendicular orientation to the bottom bulk coating is present; this could lead to a reduced adhesion and an easy removal of the thermal oxides. Substantial amounts of tiny whitish particles are observed both inside and outside

https://doi.org/10.1021/acsami.1c06061
ACS Appl. Mater. Interfaces 2021, 13, 28843−28854

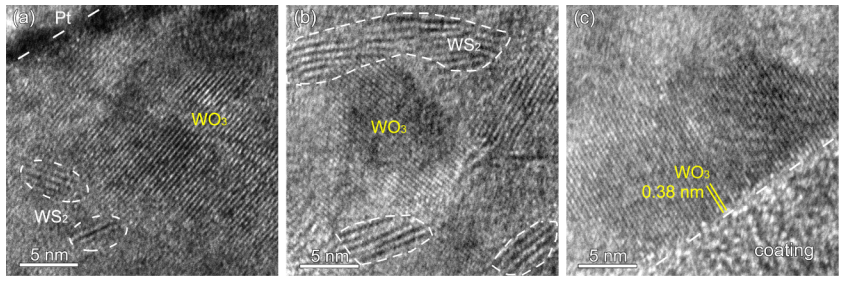

Figure 7. Cross-sectional HR-TEM images of the uneven oxidized tribofilm on the area B marked in Figure 5a: (a) top region, (b) middle region, and (c) bottom region of the tribofilm, indicating a mixture of WS_2 and WO_3 nanocrystallites formed in situ during sliding at 450 °C.

the wear track and corroborate the removal of the thermal oxides as debris (see Figures 3a,b and S2g,h). It should be pointed out that Figure 5d confirms that an about >1 μm thick coating is left below the oxidized layer on the wear track after in situ testing at 450 °C, and it is this coating that is supposed to continue to tribologically function at room temperature after cooling back down.

To further unravel the effect of oxidation, a TEM lamella was also cut by FIB from the sample annealed at 450 °C for 1 h; the corresponding HR-SEM and HR-TEM images are shown in Figure 8. Although the thermally oxidized layer on

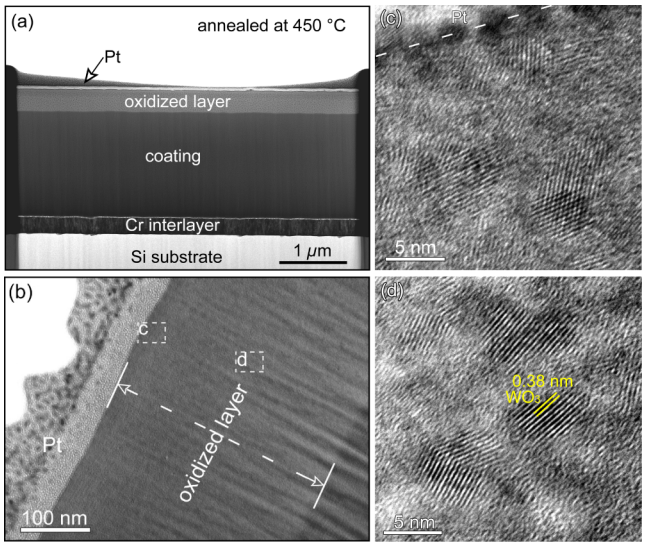

Figure 8. (a) HR-SEM image of the cross section of WS_2/a-C coating annealed at 450 °C for 1 h in the air cut out by FIB, which shows a 330 nm thick oxidized layer on the top of the unaffected underlying coating. (b) TEM image of the cross section of the oxidized layer. HR-TEM images showing a high density of newly formed WO_3(002) nanocrystallites in the oxidized layer: (c) top part and (d) middle part as marked in (b). Note that no WS_2(002) planes were observed contrarily to the oxidized tribofilm shown in Figure 7.

top of the coating could be as thick as 330 nm (Figure 8a), it was completely absent from the wear track after only 100 laps leading to ultralubrication (see Figure 2c). The removal of the oxidized layer does not compromise the integrity of the coating (about 1.6 μm thick as-deposited coating remains unaffected below the oxides, as shown in Figure 8a), which is also verified in the postannealing tribotest (see Figure 3a,b). We can therefore explain the results of the in situ tribotest, by assuming that much thinner oxidized layers (e.g., ~200 nm on the area B as revealed in Figure 6c) are more readily cleared away after formation, and their removal paves the way for replenishment of new WS_2 crystallites from the underlying bulk coating (see the center part of the wear track in Figure 3c). HR-TEM images of the top (Figure 8c) and the center (Figure 8d) of the oxidized layer confirm a homogeneous microstructure consisting of only WO_3 nanocrystallites embedded in the a-C matrix and with no WS_2 phase formed, which is different from the mixture of WS_2 and WO_3 shown in Figure 7, and suggests that when only heating without sliding, the WS_2(002) lubricating phase tends not to form.

Further confirmation of the presence of these phases comes from the SAED patterns shown in Figure S4. Figure S4a–c presents the SAED patterns of the intact thin tribofilm (a) and the partially oxidized tribofilm (b) along the cross section of the coating tribotested at 450 °C, as detailed in Figure 5. In contrast to the amorphous halo rings shown in the inset of Figure 1, Figure S4a shows that the top-most part of the intact tribofilm presents strong diffraction features of nanocrystalline WS_2 with a clear basal plane (002) orientation (two sharp symmetrical diffraction spots) along the sliding direction, in agreement with ref 5. Other WS_2 planes, such as (004), (103), (006), (200), and (205), also exist. In Figure S4b, the intensity of the WS_2(002) diffraction feature starts to dim in the oxidized layer part, and several rings assigned to WO_3 appear. WO_3 peaks dominate in the 330 nm thick-oxidized layer after annealing at 450 °C for 1 h, as shown in Figure S4c, which is in line with the HR-TEM images in Figure 8c,d. It should be pointed out, however, that Figure 8d seems to indicate that surrounding the dichalcogenide phase by the a-C matrix may mitigate the oxidation as compared to pure WS_2 films because the DLC matrix can act as a thermal and oxygen diffusion barrier. This could explain the increase in the tribological temperature threshold to ~500 °C, which is about 200 °C higher than the one reported for pure WS_2 films.[12]

The present findings of sustained ultralubrication (CoF < 0.02) up to 500 °C and reversible ultralubrication after subjecting the coating to 450 °C annealing (with 330 nm thick thermally oxidized layer) are very striking compared to what was previously reported for temperature adaptive tribocoatings. Each of these lubricious phases in the coatings studied hitherto only guarantees lubrication in a certain temperature range. Some studies directly introduced transition-metal oxides (e.g., MoO_3 and WO_3)[21,30] as potential high-temperature lubricants by employing Mo or W, alloying ingredients to favor diffusion toward the outer surface where a higher oxygen potential exists. The oxides formed replenish the consumed lubricious layer of low shear strength to mitigate friction.[39] However, in terms of friction, these attempts are not always satisfactory as molybdenum or tungsten oxides on the surface though slightly lowering the CoF to 0.5 at 500 °C, sometimes leading to

https://doi.org/10.1021/acsami.1c06061
ACS Appl. Mater. Interfaces 2021, 13, 28843−28854

unexpectedly high CoFs (0.8−1.0) at ambient temperature.[20] Similar results were reported for a MoN coating by Zhu et al.,[19] who claimed that the oxidation product MoO_3 led to an even unfavorably higher CoF than that of the as-deposited MoN coating at both room and elevated temperatures, while the sublayer oxygen-deficient oxides might be favoring slightly lower friction. Hence, oxide-based coatings are unlikely to result in ultralow friction.

As a consequence, from a design point of view, the studies on high-temperature lubrication indicate that transition-metal oxides, e.g., Magnéli phases, are an inferior choice as compared to the coatings based on TMDCs. For one thing, TMDCs are superior lubricants than their oxidized counterparts at room temperature and in the lower range above (CoF 0.02 vs >0.2); for another, the oxides can be the byproducts because of the oxidation of TMDCs when the latter are employed at high temperatures. The partially oxidized products of TMDCs and the undegraded TMDCs can act in synergy and give rise to ultralubrication below 500 °C, as seen in the results reported in Figures 2b and 7. Yet, oxides must play a secondary role in this temperature range as they tend to be dynamically removed during tribosliding, in agreement with refs 19 and 40. At ever higher temperatures, TMDCs are supposed to be completely oxidized to their TM oxides and/or related Magnéli phases, whose temporary presence can yield still acceptable CoFs increasing from 0.02 to 0.2−0.6, provided that the bulk of the coating is thermally stable.

4.2. Coating Failure above 500 °C. The remaining question is why the WS_2/a-C coating fails above 500 °C. Detailed microstructure−composition−property relationships need to be established to unravel the lubricating/failure mechanism. Figure 9 shows the surface morphologies of the WS_2/a-C coating annealed at different temperatures up to 600 °C, as revealed by SEM. Figure 9a−d all shows the typical domelike features (200 nm in diameter) of coatings produced by magnetron sputtering, with a few small whitish dots appearing on the sample annealed at 450 °C. These dots could point to a gradual local oxidation at the coating surface. In contrast, Figure 9e,f indicates that annealing at 500 °C or higher temperatures induces a structural change, resulting in smaller grains (<50 nm). In particular, the coating annealed at 600 °C becomes rather porous, tiny particles get agglomerated, and many cavities appear on the surface (associated with easy peel-off).

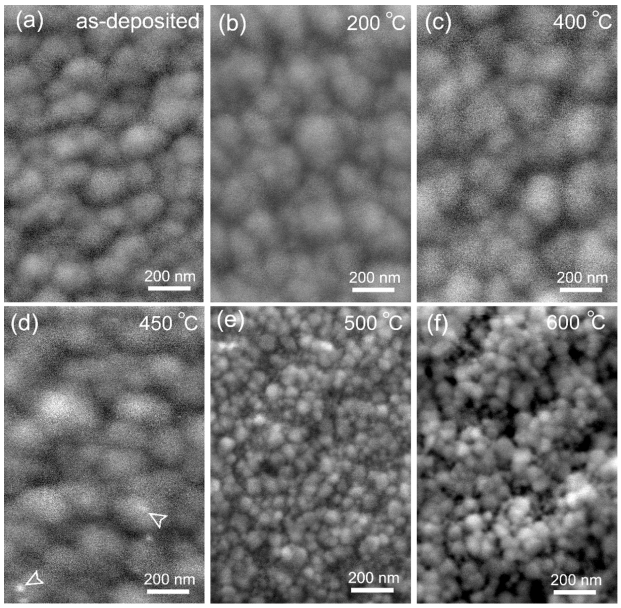

Figure 9. SEM images showing the morphologies of WS_2/a-C coatings before and after annealing at different temperatures for 1 h in air: (a) as-deposited, (b) 200 °C, (c) 400 °C, (d) 450 °C, (e) 500 °C, and (f) 600 °C.

GI-XRD of these coatings after different annealing treatments are presented in Figure S5 and show that different phases occur. In line with the microstructure analysis reported in Figure 9, the XRD spectra of the as-deposited coating and of the ones annealed at 200 and 400 °C are nearly the same. They show an asymmetrical broad (110) peak at around $2\theta = 33°$ with a long tail, which is commonly attributed to the turbostatic stacking of WS_2 basal planes.[41] Note that in a hexagonal lattice structure, the (00l) reflections correspond to the ordering in the c-direction, while the (hk0) reflections mirror the ordering in the basal planes. Provided that the coherently diffracting domains are large enough, the stacking of the $a-b$ basal lattice planes in the c direction results in a sharp peak at the position of the (100) reflection. Its tails toward larger angles signal contributions of other reflections of the (10l) family with $l = 1, 2, 3....$[42] A broad peak indicates very small coherently diffracting domains, characteristic of an amorphous structure. For the sample annealed at 450 °C, the (10l) of WS_2 becomes even broader, and a weak WO_3(200) peak at $2\theta = 24.7°$ can be seen. From 500 °C onward, the WO_3 phase dominates, indicating the complete surface oxidation of WS_2 into WO_3 when the coating is annealed above 500 °C for 1 h. The absence of the typical basal planes (002) of WS_2 at $2\theta = 14°$ in all cases suggests that WS_2 decomposes; thus, the WS_2 basal planes parallel to the coating surface that favor low friction are no longer present.

The Raman spectra of the as-deposited and annealed coatings are shown in Figure S6; weak peaks associated with the E_{1g} (~306 cm^{-1}) and A_{1g} (~421cm^{-1}) vibrational modes of WS_2[12,43] can be distinguished except for the coatings annealed at 500 and 600 °C. However, the as-deposited coating and those annealed at 200, 400, and 450 °C all present typical peaks associated with amorphous carbon; for instance, the spectral region from 1000 to 1700 cm^{-1} in the as-deposited coating can be deconvoluted into a D peak at around 1370 cm^{-1} and a G peak at 1560 cm^{-1},[33,35] which are characteristics of DLC phases. Note that the D peak is assigned to the breathing modes of sp^2 C in the rings, while the G peak is ascribed to the stretching mode of all pairs of sp^2 C both in rings and chains.[44] In contrast, for the coatings annealed at 500 and 600 °C, both WS_2 and DLC spectral features are very weak, and instead peaks at around 710 and 801 cm^{-1}, attributable to WO_3,[12] dominate the spectra, in agreement with the GI-XRD results reported in Figure S5 and the TEM results shown in Figures S7 and S8.

The SEM, XRD, and Raman results discussed above all point to a certain amount of oxidation occurring at 450 °C, which is in disagreement with the excellent triboperformance of the coating when tested while heating from room temperature to 500 °C (the coating survives >2000 laps at 500 °C). These data thus indicate some degree of the coating tolerance against oxidation during the sliding.

It is recognized that there is a significant reduction in coating hardness when the oxygen content in the coating increases and oxide phases appear. To check whether the

https://doi.org/10.1021/acsami.1c06061
ACS Appl. Mater. Interfaces 2021, 13, 28843−28854

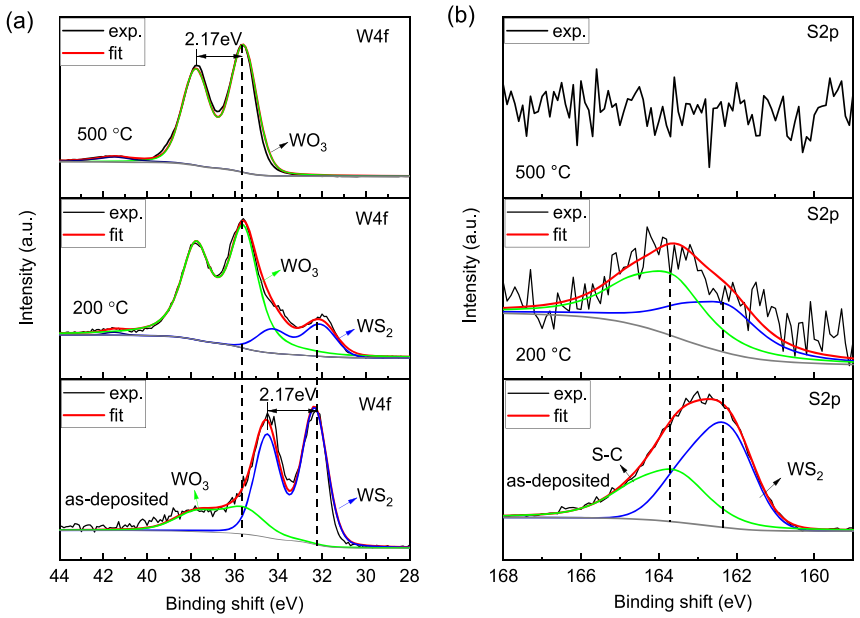

Figure 10. Typical XPS spectra of the (a) W 4f and (b) S 2p core level regions of the as-deposited WS_2/a-C coatings and of the same coatings after annealing at 200 and 500 °C, respectively.

degradation of the mechanical properties influences the adaptive tribological behavior, the nanohardness and elastic modulus of the present coating were determined by nanoindentation under different annealing conditions and are shown in Figure S7. The as-deposited coating has the highest hardness of about 12.4 GPa, and the coating annealed at 200 °C almost retains that hardness. The hardness decreased to 6−7 GPa when the coating was annealed at 400 and 450 °C. The further increase in the annealing temperature to 500 and 600 °C reduces the hardness to 3.8 and 3.3 GPa, respectively. Note that Figure 8a,b indicates that the oxidized layer is about 330 nm thick, a value larger than the indented thickness of 200 nm, implying that the latter two hardness values refer to the loose oxidized layer that mainly consists of WO_3. The modulus of the coatings tracks the decreasing trend of the hardness as a function of the annealing temperature and changes from 68 GPa for the as-deposited coating to 34 GPa for the one annealed at 600 °C. Earlier work[45] indicated that a TMDC-C coating with a hardness of >∼4 GPa is sufficient to yield a stable low-friction behavior. Consequently, the reduction in hardness (from 12.4 to 3.8 GPa) cannot explain why the coating fails above 500 °C. We propose that the annealing process indeed "softens" the WS_2/a-C coatings, and a reduced hardness aggravates the wear rates, as confirmed by the deeper wear tracks of the coatings but does not compromise coating integrity and ultralubricity. In fact, the top "softened" porous oxides in the top part of the coating get easily removed.

Figure S8 shows the TGA in air and in N_2 of the WS_2 powders removed from the target; the data confirm that WS_2 is stable up to around 500 °C in air and even up to 580 °C in dry N_2. This together with the morphology change at 500 °C induced us to explore the chemical composition of the coatings by EDS analysis; the results are listed in Table 1. For the as-deposited coating, we found about 34 atom % C, 2 atom % O, 36 atom % S, and 28 atom % W; the coating annealed at 200 °C shares a similar chemical composition with a low oxygen content, while coatings annealed at 400 and 450 °C showed a moderate decrease in sulfur to ∼25 atom %. Figure S9 shows that the increase in oxygen dovetails with the decrease in sulfur in the coatings as the annealing temperature increases. In particular, after annealing at 500 and 600 °C, the coatings present a dramatic increase in the oxygen content (>50 atom %), while sulfur is almost fully sublimed from the coating (decomposition rate of 96.1%).

These changes can be further supported by the highly surface-sensitive XPS data, as illustrated in Figure 10. The spectrum of the W 4f core level region requires two components for a good fit (Figure 10a). For the as-deposited coating, the binding energy (BE) of ∼32.1 eV[36] points to a W(4+) valence state as expected for oxygen-free WS_2, which makes up 75.5% of the coating. The detection of some W(6+) at a BE of ∼35.6 eV[46] indicates the presence of a partially oxidized phase (WO_3) on the top surface of the as-prepared coating because of contamination. For the coating annealed at 200 °C, the WO_3 contribution becomes more substantial (81.0%) in the top few nanometers of the coating analyzed by XPS. The W(4+) valence state is no longer visible in the coating annealed at 500 °C, indicating complete surface oxidation. Similarly, the sulfur S 2p peak in Figure 10b consists of two doublets, peaked at BEs of ∼162.1 and 163.5 eV and corresponding, respectively, to S−W bonds and S−C bonds;[46,47] this confirms the presence of WS_2 in the as-deposited coating. The intensity of S 2p starts to decrease when the coating was annealed at 200 °C and disappears when the coating was subjected to thermal treatment at 500 °C.

The TGA, EDS, and XPS data all point to substantial decomposition above 500 °C, confirming severe sulfur loss and a consequent decrease in the S/W ratio (Table 1). Note that sulfur content and S/M (M = W, Mo) ratios have been identified as crucial factors in TMDC-based coatings to enable the formation of enough lubricous phases for a favorable tribological behavior.[33,48] Stable ultralow CoFs of 0.02 have been observed in the range S/W = 1.33−1.79.[29] According to Table 1, the as-deposited coating and the one annealed at 200 °C have a S/W ratio of 1.30. This ratio decreases slightly to around 1.1 when the annealing temperature increases to 400

https://doi.org/10.1021/acsami.1c06061
ACS Appl. Mater. Interfaces 2021, 13, 28843−28854

and 450 °C and drops to almost zero (0.04) for the coating annealed at 500 and 600 °C. Obviously, if no more sulfur is available, the formation of WS_2 platelets is prevented. Our work[30] indicated that to realize ultralubrication, it is not necessary to reach stoichiometric WS_2 in the WS_2/a-C coatings and established a clear correlation between the S/W ratio and the CoF, where CoFs tend to be <0.05 (in dry air at room temperature) for all coatings with the S/W ratio of ≥0.95. In tribotests above 100 °C, water molecules are quickly desorbed from the sliding surfaces; this effect is equivalent to reducing the humidity level of the atmosphere. Thus, at high temperatures, the S/W ratio required to guarantee a low CoF is the one for sliding in dry air. Also, apart from the S/W ratio, a proper total content of sulfur (e.g., > 20 atom %) in the coatings is also considered essential for the formation of WS_2 phases leading to ultralow friction.[30,49]

4.3. Sustained Ultralubrication Mechanism. As far as the lubrication mechanism of TMDC-based coatings in tribology is concerned, there is ample evidence that the orientation of the basal planes of TMDC parallel to the surface in contact guarantees easy sliding.[1] This regards both surfaces in contact and hence also the in situ formed tribofilms on the wear track (see Figures 3c and S2) as well as material transferred onto the surface of the sliding counterpart (the so-called transfer film). The sliding process induces a preferred orientation in the contacting layer, so that WS_2 with basal planes oriented parallel in the tribofilm is generated during the steady state. Figure S10 illustrates that when ultralubrication conditions are achieved for the samples tested at 100, 200, 400, and 450 °C and when ramping the temperature from 100 to 500 °C, there is always a buildup of a thick transfer film on the Si_3N_4 sliding balls. Instead, for the samples tested at 500 °C, the transfer film does not form (or is more likely damaged after sliding 3000 laps), leaving the Si_3N_4 ball with a large wear scar (see Figure S10f) that corresponds to a failure). Figure S11a shows the typical Raman spectra of area 1, where an intense WS_2 spectral fingerprint characterizes the thick tribofilm, and area 2 (without visible tribofilm on the wear track) lacks the WS_2 lines. The associated EDS (Figure S11b) also confirms that some WO_3 (comprising 28.8 atom % O) has formed in the tribofilm, in agreement with the HR-TEM analysis of Figure 7.

Figure 6 confirms that under loading a thin layer of crystalline WS_2 formed in the subsurface region of the almost entirely amorphous as-deposited coating (Figure 1), tribostress is therefore essential to induce the formation of the crystalline platelets. In other words, the initial state of the WS_2/a-C coating (e.g., amorphous or crystalline, with basal planes orientated parallel or perpendicular to the sliding surface) is not a requisite for ultralubrication, in accordance with simulation results for a W−S−N coating.[50] However, whether the reordered WS_2 in the tribofilm is a newly formed material[45] made of worn coating particles or the result of the direct subsurface reorientation of the as-deposited coating material is still not clear. Scharf et al.[5] introduced two mechanisms: (a) shear-induced reorientation of perpendicular edged planes (or randomly orientated ones) and (b) an amorphous to crystalline transformation yielding basal planes parallel to the sliding direction. The former is a rotating or bending process of existing TMDC nanograins into the sliding direction. Figure 6d and the high-magnification HR-TEM images of Figure 11 indicate that WS_2 nanoplatelets tend to be newly formed at the interface: in Figure 11a, only small WS_2 platelets are

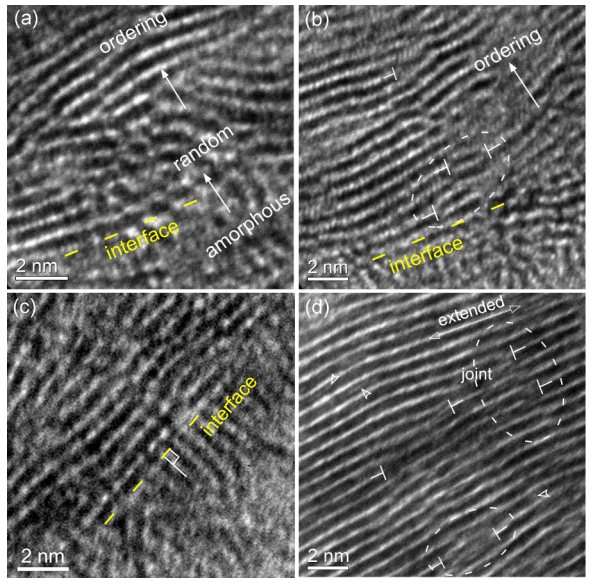

Figure 11. HRTEM micrographs illustrating the initial-stage atomic rearrangement of new WS_2(002) nanoplatelets: (a−c) several regions at the tribofilm/coating interface; the solid arrows indicate the transition from amorphous → random → ordering of WS_2(002) nanoplatelets; (d) long newly formed WS_2 platelets in the tribofilm above the interface: short WS_2 units seem to join via local geometrical defect climbing, resulting in a "reoriented" appearance. Some carbon atoms seem to be intercalated between WS_2 basal layers (see hollow arrows in (d)).

distinguished at this border, while larger crystalline platelets are present in the upper region of the tribofilm (see solid arrows). Figure 11b shows that in the tribofilm, there are fault-free localized crystalline WS_2 layers that are formed from shorter WS_2 nanoplatelets, which are joined by (partial) climbing movement (⊥). Figure 11c shows newly formed WS_2 nanoplatelets at an almost right angle to previous ones, which clearly testifies against rotation or a bending-induced reorientation mechanism. Furthermore, Figures 11d and S12 show that WS_2 nanoplatelets several nanometers away from the interface were joined into longer crystallites via unfaulting reactions because of the shear of adjacent planes, leaving "reoriented" (002) basal planes along the sliding direction. We may speculate that under frictional contact, different WS_2 units can coalesce and debond simultaneously via the dynamical atomic rearrangement (e.g., from an amorphous bulk coating). This explains why when the tribofilms get thicker than ∼100 nm, the WS_2 in the center part of the tribofilm/transfer film starts to lose its crystallinity or recover a random distribution. Some "convective-like" or "turbulent-like" densely but randomly distributed WS_2 were also reported in the middle part of the tribofilm, suggesting the occurrence of relatively easy localized sliding displacements between WS_2 nanocrystallites in the tribofilm.[33,51]

Since the location of the contact spots changes with time and material may be transported, squeezed, and flattened, the tribofilm in sliding contact is dynamic instead of static. During the atomic rearrangements in the WS_2 nanocrystals parallel to the sliding direction, the dangling or unsaturated bonds at the edge of WS_2 basal planes will react with ambient oxygen to form tribo-oxidation products such as WO_3. A high-temperature environment could facilitate the oxidizing process (illustrated by ∼330 nm/L h at 450 °C in Figure 8a);

https://doi.org/10.1021/acsami.1c06061
ACS Appl. Mater. Interfaces 2021, 13, 28843−28854

however, a consequent increase in friction will not occur if the coating keeps its integrity and retains enough sulfur content (<500 °C).

Most of the carbon is released from the contact[33,35] during sliding and turns into debris on the sides of the wear track, while a few carbon atoms intercalate between WS_2 planes (see hollow arrows in Figure 11d) and cause the lattice to expand.

Figure 12 shows the schematics of the adaptive tribological mechanism of WS_2/a-C coating at high temperatures. This

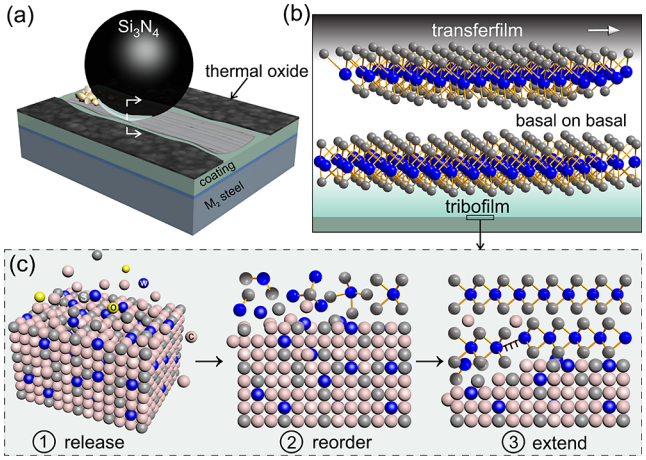

Figure 12. Schematics of the adaptive tribological mechanism of a WS_2/a-C coating at high temperature (not to scale). The transition from the running-in to ultralubricity involves the dynamical removal of the thermally oxidized layer and the replenishment of lubricating tribofilms at the wear track as well as of a transferfilm adhering to the Si_3N_4 counterpart ball (a). These events trigger a nondirect contact where the rearrangement of atoms into the WS_2(002) basal planes forms a self-assembled basal plane on the basal plane lubricating tribocouple (b). (c) Selective rearrangement of WS_2 units via localized geometrical defects (⊥) dynamically at the wear interface from the as-prepared amorphous bulk coating. Note the colored atoms are blue—tungsten, gray—sulfur, yellow—oxygen, and pink—carbon.

self-adaption under high-temperature conditions is associated with a dynamical removal of surface asperities, native and in situ formed oxide layers, and continuous buildup and wear off of tribofilm/transferfilm. The coating gets oxidized initially, but the oxidized layer will be swiftly removed during sliding (Figure 12a); meanwhile, the lubricating tribofilm at the wear track and the transfer film adhering to the Si_3N_4 counterpart ball are dynamically formed, establishing a nondirect contact in between self-assembled WS_2, which constitute the new lubricating tribocouple (Figure 12b). Note that at relatively higher temperatures, oxidation and fast removal of the oxidized layers coincide, keeping an ultralow CoF of 0.02 at <500 °C (provided the removal rate of oxides is faster than the oxidation rate of the coating and the bottom coating retains its structural integrity as to allow for the replenishment of WS_2). Figure 12c describes the formation and selective rearrangement of WS_2 units via unfaulting reactions (⊥) at the wear interface from the as-deposited amorphous bulk coating. This is accompanied by the release of the carbon from the contact as well as small units of WS_2 becoming ordered and joining until a continuous WS_2 film with basal planes parallel to the sliding direction is formed. Above 500 °C, sulfur loss becomes severe, causing insufficient sulfur supply for the formation of WS_2. The coating also starts to decompose thereafter and becomes porous and easy to peel off. All of these result in high friction and coating failure.

5. CONCLUSIONS

This study reports an ultralow friction, thermally resistant WS_2/a-C coating produced by magnetron sputtering, which can provide reversible structural and chemical self-adaptations to a broad range of ambient environmental conditions. The key findings are summarized below:

(1) This chameleon-like tribocoating retains an ultralow CoF (0.02) from room temperature to elevated temperature up to 500 °C; it also exhibits reversible triboperformance at room temperature after annealing to 450 °C.

(2) Oxides (e.g., WO_3) formed at elevated temperature play a minor role in lubrication as the oxidized surface layer is removed dynamically during sliding. Instead, severe sulfur loss and degraded thermal stability of the coating itself account for the coating failure above 500 °C.

(3) The WS_2 nanocrystallites form via selective atomic rearrangement from the amorphous bulk and join into longer crystallites because of defect climbing driven by frictional contact; these crystallites account for the stable ultralubrication. The initial orientation of WS_2 in the as-deposited coating does not influence the formation of well-functioning WS_2 tribofilms that result in ultralow friction.

(4) The CoF is temperature independent until the coating thermally degrades above 500 °C, which makes this WS_2/a-C coating a promising candidate for aerospace applications requiring long-lasting, stable ultralubricity over a broad range of temperatures.

■ ASSOCIATED CONTENT

Supporting Information

The Supporting Information is available free of charge at https://pubs.acs.org/doi/10.1021/acsami.1c06061.

Figure S1, In situ triboperformance of the WS_2/a-C coating at different discrete temperatures; Figure S2, SEM micrographs showing the wear track morphologies after the tribotests for 5000 laps at different testing temperatures; Figure S3, SEM micrographs showing the morphology of residual coating after in situ tribotesting at 500 °C; Figure S4, SAED patterns of (a) the intact tribofilm (b) oxidized tribofilm on the wear track of the WS_2/a-C nanocomposite coating tribotested at 450 °C and (c) the same coating annealed in air at 450 °C for 1 h; Figure S5, GI-XRD spectra of the WS_2/a-C coating after different annealing treatments; Figure S6, Raman spectra of the WS_2/a-C coating after annealing at different temperatures; Figure S7, Nanohardness (H) and elastic modulus (E) of the WS_2/a-C coating determined from nanoindentation at different annealing temperatures; Figure S8, TGA under different gas conditions of pure WS_2 powders taken from the target used for the sputtering deposition; Figure S9, typical EDS data indicating an increase in the O content and a decrease in the S content of the WS_2/a-C coating after annealing at different temperatures; Figure S10, optical microscopy images of the ball scars after tribo-sliding under different conditions; Figure S11, typical Raman spectra and indicative EDS spectra; Figure S12, HR-TEM images (PDF)

https://doi.org/10.1021/acsami.1c06061
ACS Appl. Mater. Interfaces 2021, 13, 28843−28854

AUTHOR INFORMATION

Corresponding Authors

Huatang Cao − *Engineering and Technology Institute Groningen, University of Groningen, Groningen 9747 AG, The Netherlands; Henry Royce Institute, Department of Materials, University of Manchester, Manchester M13 9PL, U.K.;* orcid.org/0000-0002-3706-3035; Email: huatang.cao@manchester.ac.uk

Ping Xiao − *Henry Royce Institute, Department of Materials, University of Manchester, Manchester M13 9PL, U.K.;* orcid.org/0000-0002-6063-3681; Email: p.xiao@manchester.ac.uk

Authors

Jamo Momand − *Zernike Institute for Advanced Materials, University of Groningen, Groningen 9747 AG, The Netherlands;* orcid.org/0000-0001-5153-2427

Ali Syari'ati − *Zernike Institute for Advanced Materials, University of Groningen, Groningen 9747 AG, The Netherlands;* orcid.org/0000-0003-0161-8980

Feng Wen − *Engineering and Technology Institute Groningen, University of Groningen, Groningen 9747 AG, The Netherlands;* orcid.org/0000-0001-5018-9372

Petra Rudolf − *Zernike Institute for Advanced Materials, University of Groningen, Groningen 9747 AG, The Netherlands;* orcid.org/0000-0002-4418-1769

Jeff Th. M. De Hosson − *Zernike Institute for Advanced Materials, University of Groningen, Groningen 9747 AG, The Netherlands;* orcid.org/0000-0002-2587-3233

Yutao Pei − *Engineering and Technology Institute Groningen, University of Groningen, Groningen 9747 AG, The Netherlands;* orcid.org/0000-0002-1817-2228

Complete contact information is available at: https://pubs.acs.org/10.1021/acsami.1c06061

Notes

The authors declare no competing financial interest.

ACKNOWLEDGMENTS

The authors thank Prof. Wesley Browne of the Stratingh Institute of the University of Groningen for support with Raman spectroscopy as well as Dr. Qiangli Lu and Dr. Amar M. Kamat of the Engineering and Technology Institute Groningen for help with the TGA analysis and the annealing treatment, respectively. Partial financial support came from the Advanced Materials research program of the Zernike National Research Centre under the Bonus Incentive Scheme (BIS) of the Dutch Ministry for Education, Culture and Science. F.W. from Hainan University, China, thanks for the grant in the visiting scholar scheme.

REFERENCES

(1) Muratore, C.; Voevodin, A. A. Chameleon Coatings: Adaptive Surfaces to Reduce Friction and Wear in Extreme Environments. *Annu. Rev. Mater. Res.* **2009**, *39*, 297−324.

(2) Voevodin, A. A.; Zabinski, J. S. Supertough Wear-Resistant Coatings with "Chameleon" Surface Adaptation. *Thin Solid Films* **2000**, *370*, 223−231.

(3) Sliney, H. E. Solid Lubricant Materials for High Temperatures-A Review. *Tribol. Int.* **1982**, *15*, 303−315.

(4) Aouadi, S. M.; Luster, B.; Kohli, P.; Muratore, C.; Voevodin, A. A. Progress in the Development of Adaptive Nitride-Based Coatings for High Temperature Tribological Applications. *Surf. Coat. Technol.* **2009**, *204*, 962−968.

(5) Scharf, T. W.; Kotula, P. G.; Prasad, S. V. Friction and Wear Mechanisms in MoS_2/Sb_2O_3/Au Nanocomposite Coatings. *Acta Mater.* **2010**, *58*, 4100−4109.

(6) Gharam, A. A.; Lukitsch, M. J.; Balogh, M. P.; Irish, N.; Alpas, A. T. High Temperature Tribological Behavior of W-DLC against Aluminum. *Surf. Coat. Technol.* **2011**, *206*, 1905−1912.

(7) Polcar, T.; Evaristo, M.; Cavaleiro, A. The Tribological Behavior of W-S-C films in Pin-on-Disk Testing at Elevated Temperature. *Vacuum* **2007**, *81*, 1439−1442.

(8) Hu, J. J.; Bultman, J. E.; Muratore, C.; Phillips, B. S.; Zabinski, J. S.; Voevodin, A. A. Tribological Properties of Pulsed Laser Deposited Mo-S-Te Composite Films at Moderate High Temperatures. *Surf. Coat. Technol.* **2009**, *203*, 2322−2327.

(9) Liu, C. C.; Chen, L.; Zhou, J. S.; Zhou, H. D.; Chen, J. M. Tribological Properties of Adaptive Phosphate Composite Coatings with Addition of Silver and Molybdenum Disulfide. *Appl. Surf. Sci.* **2014**, *300*, 111−116.

(10) Zeng, C.; Pu, J. B.; Wang, H. X.; Zheng, S. J.; Wang, L. P.; Xue, Q. J. Study on Atmospheric Tribology Performance of MoS_2-W Films with Self-Adaption to Temperature. *Tribol. Int.* **2019**, *45*, 15834−15842.

(11) Aouadi, S. M.; Singh, D. P.; Stone, D. S.; Polychronopoulou, K.; Nahif, F.; Rebholz, C.; Muratore, C.; Voevodin, A. A. Adaptive VN/Ag Nanocomposite Coatings with Lubricious Behavior from 25 to 1000 °C. *Acta Mater.* **2010**, *58*, 5326−5331.

(12) Scharf, T. W.; Rajendran, A.; Banerjee, R.; Sequeda, F. Growth, Structure and Friction Behavior of Titanium Doped Tungsten Disulphide (Ti-WS_2) Nanocomposite Thin Films. *Thin Solid Films* **2009**, *517*, 5666−5675.

(13) Gupta, S.; Filimonov, D.; Palanisamy, T.; El-Raghy, T.; Barsoum, M. W. Ta_2AlC and Cr_2AlC Ag-based Composites-New Solid Lubricant Materials for Use over a Wide Temperature Range against Ni-Based Superalloys and Alumina. *Wear* **2007**, *262*, 1479−1489.

(14) Aouadi, S. M.; Paudel, Y.; Simonson, W. J.; Ge, Q.; Kohli, P.; Muratore, C.; Voevodin, A. A. Tribological Investigation of Adaptive Mo_2N/MoS_2/Ag Coatings with High Sulfur Content. *Surf. Coat. Technol.* **2009**, *203*, 1304−1309.

(15) Shtansky, D. V.; Bondarev, A. V.; Kiryukhantsev-korneev, P. V.; Rojas, T. C.; Godinho, V.; Fernández, A. Structure and Tribological Properties of MoCN-Ag Coatings in the Temperature Range of 25−700 °C. *Appl. Surf. Sci.* **2013**, *273*, 408−414.

(16) Ouyang, J. H.; Sasaki, S.; Murakami, T.; Umeda, K. Tribological Properties of Spark-Plasma-Sintered $ZrO_2(Y_2O_3)$-CaF-Ag Composites at Elevated Temperatures. *Wear* **2005**, *258*, 1444−1454.

(17) Muratore, C.; Hu, J. J.; Voevodin, A. A. Tribological Coatings for Lubrication over Multiple Thermal Cycles. *Surf. Coat. Technol.* **2009**, *203*, 957−962.

(18) Dai, X.; Wen, M.; Wang, J.; Cui, X.; Wang, X.; Zhang, K. The Tribological Performance at Elevated Temperatures of MoNbN-Ag Coatings. *Appl. Surf. Sci.* **2020**, *509*, No. 145372.

(19) Zhu, X. D.; Yue, D.; Shang, C.; Fan, M. T.; Hou, B. Phase Composition and Tribological Performance of Molybdenum Nitride Coatings Synthesized by IBAD. *Surf. Coat. Technol.* **2013**, *228*, S184−S189.

(20) Debnárová, S.; Souček, P.; Vašina, P.; Zábranský, L.; Buršíková, V.; Mirzaei, S.; Pei, Y. T. The Tribological Properties of Short Range Ordered W-B-C Protective Coatings Prepared by Pulsed Magnetron Sputtering. *Surf. Coat. Technol.* **2019**, *357*, 364−371.

(21) Chen, Z. S.; Li, H. J.; Fu, Q. G.; Qiang, X. F. Tribological Behaviors of SiC/h-BN Composite Coating at Elevated Temperatures. *Tribol. Int.* **2012**, *56*, 58−65.

(22) Muratore, C.; Voevodin, A. A.; Hu, J. J.; Zabinski, J. S. Tribology of Adaptive Nanocomposite Yttria-Stabilized Zirconia Coatings Containing Silver and Molybdenum from 25 to 700 °C. *Wear* **2006**, *261*, 797−805.

(23) Zhang, X.; Luster, B.; Church, A.; Muratore, C.; Voevodin, A. A.; Kohli, P.; Aouadi, S.; Talapatra, S. Carbon Nanotube−MoS_2 Composites as Solid Lubricants. *ACS Appl. Mater. Interfaces* **2009**, *1*, 735−739.
(24) Bondarev, A. V.; Kiryukhantsev-korneev, P. V.; Sidorenko, D. A.; Shtansky, D. V. A New Insight into Hard Low Friction MoCN−Ag Coatings Intended for Applications in Wide Temperature Range. *Mater. Des.* **2016**, *93*, 63−72.
(25) Tillmann, W.; Wittig, A.; Stangier, D.; Moldenhauer, H.; Thomann, C. A.; Debus, J.; Aurich, D.; Bruemmer, A. Temperature-Dependent Tribological Behavior of MoS_x Thin Films Synthesized by HiPIMS. *Tribol. Int.* **2021**, *153*, 106655−106660.
(26) Wahl, K. J.; Seitzman, L. E.; Bolster, R. N.; Singer, I. L.; Peterson, M. B. Ion-Beam Deposited Cu-Mo Coatings as High Temperature Solid Lubricants. *Surf. Coat. Technol.* **1997**, *89*, 245−251.
(27) Gulbiński, W.; Suszko, T. Thin Films of MoO_3-Ag_2O Binary Oxides-the High Temperature Lubricants. *Wear* **2006**, *261*, 867−873.
(28) Pei, Y. T.; Galvan, D.; De Hosson, J. T. M. Tribological Behavior and Thermal Stability of TiC/a-C:H Nanocomposite Coatings. *J. Vac. Sci. Technol., A.* **2006**, *24*, 1448−1453.
(29) Cao, H. T.; De Hosson, J. T. M.; Pei, Y. T. Effect of Carbon Concentration and Argon Flow Rate on the Microstructure and Triboperformance of Magnetron Sputtered WS_2/a-C Coatings. *Surf. Coat. Technol.* **2017**, *332*, 142−152.
(30) Cao, H. T.; Wen, F.; Kumar, S.; Rudolf, P.; De Hosson, J. T. M.; Pei, Y. T. On the S/W Stoichiometry and Triboperformance of WS_xC(H) Coatings Deposited by Magnetron Sputtering. *Surf. Coat. Technol.* **2019**, *365*, 41−51.
(31) Cao, H. T.; Wen, F.; De Hosson, J. T. M.; Pei, Y. T. Instant WS_2 Platelets Reorientation of Self-Adaptive WS_2/a-C Tribocoating. *Mater. Lett.* **2018**, *229*, 64−67.
(32) Ju, H. B.; Jia, P.; Xu, J. H.; Yu, L. H.; Asempah, I.; Geng, Y. X. Crystal Structure and High Temperature Tribological Behavior of Niobium Aluminum Nitride Films. *Materialia* **2018**, *3*, 202−211.
(33) Cao, H. T.; Wen, F.; De Hosson, J. T. M.; Pei, Y. T. On the Self-Repair of WS_2/a-C Tribocoating. *Adv. Mater. Interfaces* **2020**, *7*, 1900938−1900953.
(34) Nyberg, H.; Sundberg, J.; Särhammar, E.; Gustavsson, F.; Kubart, T.; Nyberg, T.; Jansson, U.; Jacobson, S. Extreme Friction Reductions During Initial Running-in of W-S-C-Ti Low-Friction Coatings. *Wear* **2013**, *302*, 987−997.
(35) Xu, J.; He, T. F.; Chai, L. Q.; Qiao, L.; Zhang, X. Q.; Wang, P.; Liu, W. M. Selective-releasing-affected Lubricant Mechanism of a Self-assembled MoS_2/Mo−S−C Nanoperiod Multilayer Film Sliding in Diverse Atmospheres. *Phys. Chem. Chem. Phys.* **2017**, *19*, 8161−8173.
(36) Sundberg, J.; Nyberg, H.; Särhammar, E.; Gustavsson, F.; Kubart, T.; Nyberg, T.; Jacobson, S.; Jansson, U. Influence of Ti Addition on the Structure and Properties of Low-Friction W-S-C coatings. *Surf. Coat. Technol.* **2013**, *232*, 340−348.
(37) Bhowmick, S.; Lou, M.; Khan, M. Z. U.; Banerji, A.; Alpas, A. T. Role of an Oxygen Atmosphere in High Temperature Sliding Behaviour of W Containing Diamond-Like Carbon (W-DLC). *Surf. Coat. Technol.* **2017**, *332*, 399−407.
(38) Greenwood, O. D.; Moulzolf, S. C.; Blau, P. J.; Lad, R. J. The Influence of Microstructure on Tribological Properties of WO_3 Thin Films. *Wear* **1999**, *232*, 84−90.
(39) Erdemir, A. A Crystal-Chemical Approach to Lubrication by Solid Oxides. *Tribol. Lett.* **2000**, *8*, 97−102.
(40) Suszko, T.; Gulbiński, W.; Jagielski, J. The Role of Surface Oxidation in Friction Processes on Molybdenum Nitride Thin Films. *Surf. Coat. Technol.* **2005**, *194*, 319−324.
(41) Regula, M.; Ballif, C.; Moser, J. H.; Lévy, F. Structural, Chemical, and Electrical Characterisation of Reactively Sputtered WS_x Thin Films. *Thin Solid Films* **1996**, *280*, 67−75.
(42) Weise, G.; Mattern, N.; Hermann, H.; Teresiak, A.; Bächer, I.; Brückner, W.; Bauer, H. D.; Vinzelberg, H.; Reiss, G.; Kreissig, U.; Mäder, M.; Markschläger, P. Preparation, Structure and Properties of MoS_x Films. *Thin Solid Films* **1997**, *298*, 98−106.
(43) Polcar, T.; Gustavsson, F.; Thersleff, T.; Jacobson, S.; Cavaleiro, A. Complex Frictional Analysis of Self-Lubricant W-S-C/Cr Coating. *Faraday Discuss.* **2012**, *156*, 383−401.
(44) Ferrari, A. C. Determination of Bonding in Diamond-Like Carbon by Raman Spectroscopy. *Diamond Relat. Mater.* **2002**, *11*, 1053−1061.
(45) Polcar, T.; Cavaleiro, A. Review on Self-Lubricant Transition Metal Dichalcogenide Nanocomposite Coatings Alloyed with Carbon. *Surf. Coat. Technol.* **2011**, *206*, 686−695.
(46) Moulder, J. F.; Stickle, W. F.; Sobol, P. E. *Handbook of X-Ray Photoelectron Spectroscopy*; Physical Electronics Division, Perkin-Elmer Corp.: Eden Prairie, Minnesota, USA, 1993.
(47) Pimentel, J. V.; Polcar, T.; Evaristo, M.; Cavaleiro, A. Examination of the Tribolayer Formation of A Self-Lubricant WSC Sputtered Coating. *Tribol. Int.* **2012**, *47*, 188−193.
(48) Vuchkov, T.; Evaristo, M.; Yaqub, T. B.; Polcar, T.; Cavaleiro, A. Synthesis, Microstructure and Mechanical Properties of W−S−C Self-Lubricant Thin Films Deposited by Magnetron Sputtering. *Tribol. Int.* **2020**, *150*, 106363−106376.
(49) Voevodin, A. A.; O'Neill, J. P.; Zabinski, J. S. Nanocomposite Tribological Coatings for Aerospace Applications. *Surf. Coat. Technol.* **1999**, *116−119*, 36−45.
(50) Isaeva, L.; Sundberg, J.; Mukherjee, S.; Pelliccione, C. J.; Lindblad, A.; Segre, C. U.; Jansson, U.; Sarma, D. D.; Eriksson, O.; Kádas, K. Amorphous W-S-N Thin Tilms: The Atomic Structure behind Ultra-Low Friction. *Acta Mater.* **2015**, *82*, 84−93.
(51) Cao, H. T.; De Hosson, J. T. M.; Pei, Y. T. Self-Healing of a Pre-Notched WS_2/a-C Coating. *Mater. Res. Lett.* **2019**, *7*, 103−109.

https://doi.org/10.1021/acsami.1c06061
ACS Appl. Mater. Interfaces 2021, 13, 28843−28854